RSC Advances

PAPER

View Article Online
View Journal | View Issue



Cite this: *RSC Adv.*, 2026, **16**, 10012

# Growth and morphological control of metastable KDP crystals using defect-free seeds

Chixuan Li, Chengqian Zhang and Yan Ren *

Many functional crystal materials with significant practical value belong to metastable phases. However, the controllable growth of metastable crystals, compared with their thermodynamically stable crystalline phases, faces substantial technical bottlenecks, primarily attributed to their tendency to transform into their stable phases. Herein, we demonstrate that defect-free microscale seeds of a metastable phase, which possess smooth surfaces and high intrinsic two-dimensional (2D) nucleation barriers, can effectively suppress undesirable phase transformations, thereby realizing controlled growth and morphological regulation of the metastable phase. We employ a solution-seeding method to precisely determine the solubility of the metastable monoclinic phase of potassium dihydrogen phosphate ($KH_2PO_4$, KDP) and the critical supersaturation for initiating growth on its distinct crystal faces. This allows for the clear delineation of the growth regions for the stable tetragonal and metastable monoclinic phases of KDP. By controlling supersaturation and growth kinetics within the stable zone of the tetragonal phase, we further achieve the growth of the monoclinic phase with precise morphological control, producing one-dimensional (1D) single crystal fibers (SCFs) and three-dimensional (3D) rod-shaped crystals. This study provides a methodology for investigating the growth and morphological control of metastable crystalline phases and is expected to strongly support the exploration and development of new metastable-phase functional crystalline materials for advanced device applications.

Received 23rd December 2025
Accepted 5th February 2026

DOI: 10.1039/d5ra09916a

rsc.li/rsc-advances



## Introduction

Many metastable crystalline phases possess physicochemical properties superior to their stable counterparts. These materials find broad applications across diverse fields, including nonlinear optics,[1] optoelectronics,[2–4] pharmaceuticals,[5,6] catalysis,[7] ceramics,[8] energy storage,[9] and biology.[10] Discovering and developing novel metastable-phase crystals represent a promising avenue for innovation in materials science. Meanwhile, controlled crystal growth is a key technology for developing high-performance metastable materials, and precise morphological control of the crystalline product is critical in this process as it directly influences the performance of crystalline materials in key applications such as pharmaceutical bioavailability, catalytic efficiency, photoelectric conversion efficiency and material mechanical strength.[11]

A metastable phase represents the state of a material that is not at its global free energy minimum but is rather trapped in a local minimum, possessing higher Gibbs free energy than that of the thermodynamically stable phase under the same conditions.[12] Its persistence is kinetically controlled by relying on an energy barrier that hinders transformation to the stable phase.[13] According to the Ostwald's rule of stages,[14–16] crystallization from solutions often starts with thermodynamically unstable phases, gradually transforming to thermodynamically stable phases. Consequently, under appropriate conditions and with sufficient crystallization time, the stable polymorph is readily obtained due to its thermodynamic stability. However, the intrinsic instability of metastable polymorphs makes investigation into their crystal growth extremely challenging.[17] Currently, there is a lack of effective methods to successfully determine the thermodynamic and kinetic parameters for the crystal growth of metastable phases to achieve the growth and morphological control of high-quality metastable phase crystals.[18,19]

Potassium dihydrogen phosphate ($KH_2PO_4$, KDP) crystals usually work as the model for theoretical studies on crystal growth.[20] Recently, significant focus has been placed on research regarding the competitive nucleation and growth of the stable tetragonal phase ($I\bar{4}2d$) and metastable monoclinic phase ($P2_1/c$) of KDP.[21–23] Several studies have indicated that the metastable monoclinic phase of KDP is more competitive in nucleation in highly supersaturated solutions due to its lower interfacial energy and structural similarity with the solution.[24–26] However, accurately determining the solubility curve of metastable KDP crystals remains a challenge, which not only impedes the precise calculation of the crystal–liquid interfacial free energy but also hinders the understanding of nucleation and growth mechanisms for metastable polymorphs. Our

*State Key Laboratory of Crystal Materials, Shandong University, Jinan 250100, China. E-mail: ry@sdu.edu.cn*

previous work investigated the growth of thermodynamically stable tetragonal KDP single-crystal fibers (SCFs) using defect-free fiber seeds.[27] The growth of these defect-free, fibrous crystals at high supersaturation was found to follow a two-dimensional (2D) nucleation mechanism on smooth crystal faces rather than the dislocation growth mechanism. The classic crystal growth theory demonstrates that smooth crystal faces significantly enhance the energy barrier for 2D nucleation.[28–30] This characteristic suggests that defect-free metastable crystal seeds may also exhibit increased resistance to phase transformations. If this reasoning is valid, it will enable the investigation of the thermodynamics and growth kinetics of metastable-phase crystals in highly supersaturated solutions using defect-free crystal seeds.

In this article, we first evaluated the thermodynamic conditions for the nucleation and growth of metastable monoclinic KDP crystals and determined the critical supersaturation ratio for metastable phase nucleation in deeply undercooled solutions. Subsequently, the solubility and growth curves were measured using micron-sized defect-free fiber seeds *via* the conventional solution-seeding method. This clarified the critical supersaturation required to initiate growth for both the stable and metastable crystals. Furthermore, the delineated crystal growth phase regions indicated that within the stable region of the tetragonal crystal phase, the defect-free monoclinic phase can co-exist metastably and its seeded growth can be fully controlled. Finally, the accurate morphological control of the metastable phase is realized by regulating the growth kinetics of individual crystal faces to obtain 1D SCFs with large length-to-width ratio and 3D rod-shaped crystals.

## Experimental

### Materials

Potassium dihydrogen phosphate (KDP) with a purity of 99.9% was used, which is specially produced for the growth of research-grade crystals for high-power laser applications. The ultrapure water was provided by a Merck water purifier (Milli-Q Reference).

Different concentrations of KDP solutions were prepared by dissolving KDP microcrystals in ultrapure water. Specifically, a solution of 35 g KDP/100 g $H_2O$ was used to crystallize metastable monoclinic fiber seeds *via* spontaneous nucleation. For the growth kinetics studies, a series of solutions with concentrations of 43, 44, 45, 46, 47, and 48 g KDP/100 g $H_2O$ were employed. All solutions were overheated at 80 °C for 48 hours to ensure complete dissolution and then filtered through a 0.22-μm membrane filter. The filtrate was cooled to room temperature, sealed and stored for subsequent use.

### Powder X-ray diffraction (PXRD)

To further distinguish the two phases, PXRD measurements were conducted using a Rigaku SmartLab-9 KW diffractometer with Cu Kα radiation ($\lambda = 1.5418$ Å). Data over the range of 10°–50° in $2\theta$ were collected with a scanning step of 0.02° and a continuous scan rate of 20° $min^{-1}$ at an ambient temperature.

### Atomic force microscopy (AFM)

The surface micro morphologies of metastable monoclinic KDP fiber seeds of different sizes were obtained using a Bruker Dimension Icon atomic force microscope in the tapping mode. The selected-area profiles of the prismatic surfaces were analyzed using the NanoScope Analysis software. All crystals were freshly prepared for AFM measurement.

### Scanning electron microscopy (SEM)

SEM images of the monoclinic KDP crystals were taken using a Hitachi SU-8010 ultrahigh-resolution field-emission scanning electron microscope at an accelerating voltage of 5.0 kV, and the samples were Au-sputtered.

## Results and discussion

### Nucleation of metastable monoclinic KDP

The critical supersaturation ratio required for metastable monoclinic KDP crystal nucleation was first evaluated. Achieving a highly supersaturated solution is challenging due to its inherent instability.[31] A previous work achieved highly supersaturated KDP solutions by using electrostatically levitated droplets (1–8 μL (ref. 22)) or evaporating microdroplets suspended in oil (less than 1 nL (ref. 23)), thereby facilitating the formation of metastable phases. Herein, to be compatible with standard crystal growth operations in the laboratory, we nevertheless employed conventional methods and glass vials to prepare highly supersaturated solutions for crystallization. Typically, saturated solutions at temperatures higher than 60 °C were prepared and then filtered and maintained at 0 °C for 24 hours to achieve high-purity solutions with high supersaturations. The preparation of high-purity solutions was essential to avoid impurity-induced crystallization under high supersaturation. These undercooled solutions exhibit a remarkably high stability and do not spontaneously nucleate in the absence of external disturbances. To observe the nucleation, mechanical shaking (*e.g.*, vial tapping) was then applied to break the metastable equilibrium. As nucleation relies on thermal fluctuations within the solution,[32] the inhomogeneous flow caused by shaking promotes nuclei formation. At a supersaturation ratio $S_T$ (relative to the tetragonal phase of KDP) of 2.96 (corresponding to undercooling at 61 °C), microcrystals were formed by shaking (Fig. 1a). The resulting crystalline phase was identified *via* XRD analysis. The discrepancy in the relative peak intensities in the diffraction pattern shown in Fig. 1b is attributed to the strong preferred orientation of the substrate-grown microcrystals during the *in situ* measurement, as well as the influence of the solution environment. Nevertheless, the measured diffraction peak positions are consistent with the stimulated ones, confirming that the phase is tetragonal. When the suspension was taken out from the 0 °C environment and observed under a microscope at ambient temperature (25 °C ± 2 °C), these small crystals continued to grow into large blocky crystals with a distinct tetragonal phase (Fig. 1c). Therefore, the crystals formed in the solution of $S_T = 2.96$ were identified as the thermodynamically stable tetragonal phase. In contrast,

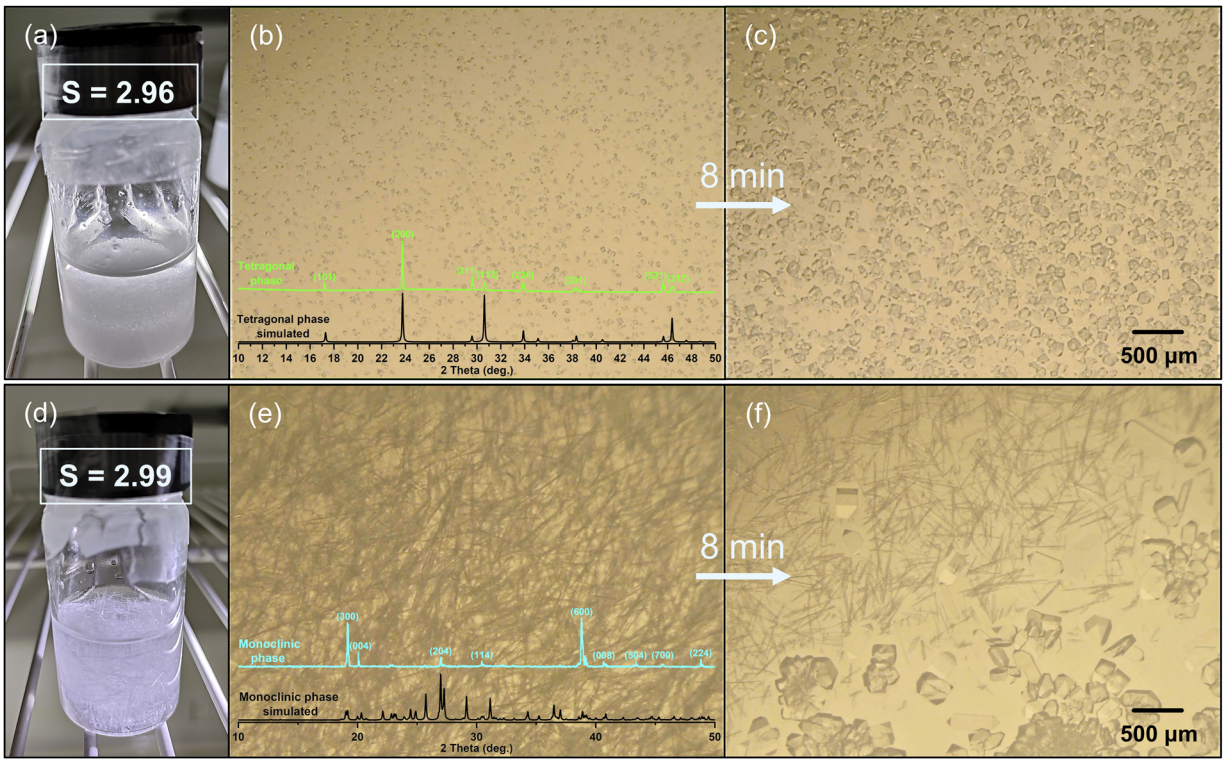


Fig. 1 *In situ* observation of the crystallization behavior of KDP solutions at different supersaturation ratios ($S_T$) relative to the tetragonal phase: (a) and (d) initial crystals formed at $S_T = 2.96$ and $S_T = 2.99$, respectively. (b) and (e) Micrographs and XRD patterns of the initial crystals. (c) and (f) Corresponding morphological evolution within 8 minutes as supersaturation decreases due to an increase in temperature.

fibrous crystals nucleate at $S_T = 2.99$ (corresponding to undercooling at 62 °C) (Fig. 1d). XRD showed that the original structure of these fibers belongs to the monoclinic phase (Fig. 1e). When the crystallizing solution was taken out from the 0 °C environment for observation, the fibrous crystals immediately dissolved and transformed into bulk crystals with a bipyramidal morphology (Fig. 1f). Obviously, a crystal transition occurred herein due to the metastability of the monoclinic crystal and its high solubility. The crystals transformed from the original monoclinic phase into the tetragonal phase. In the above experiments, low temperature significantly reduced the nucleation rate, stabilized the solution, and made it possible to achieve a solution with an extremely high supersaturation ratio. This experiment indicates that a solution with high supersaturation is a prerequisite for metastable monoclinic phase nucleation. This is precisely why the metastable monoclinic phase of KDP has not been identified for many years in the conventional preparation of KDP crystals, leading people to believe that unlike DKDP crystals, KDP could not form a monoclinic phase in aqueous solution under ambient conditions.[33]

### Methodology for realizing the controlled growth of the metastable phase

To conduct the thermodynamics and kinetics study and realize the controlled growth of metastable crystals, it is essential to clarify the saturation curve of the metastable phase, the solubility difference between the metastable phase and the stable phase, and the feasibility of growing crystals under metastable conditions. As described above, the tendency for solution-mediated transformation from the metastable phase to the stable phase makes it difficult to accurately evaluate the growth thermodynamics. However, we found that the apparent stability of metastable phases in a solution actually depends on whether the crystals are defect-free. It was observed that under dynamically changing temperature conditions when observing the critical state of solute dissolution or crystallization in the solution, low-quality, defective metastable crystal seeds tend to transition to the stable phase, whereas high-quality ones do not (see Fig. S1 and SI Movie 1). No crystal transition occurs on the surface of a high-quality fiber crystal. This characteristic of high-quality fiber seeds makes it possible to study the thermodynamics, kinetics and controlled crystal growth of metastable crystals.

A polarized microscope observation indicated that there are quite a few perfect metastable fiber crystals with no apparent macroscopic defects formed by a rapid spontaneous crystallization in highly supersaturated droplets. Atomic force microscopy (AFM) was used to observe the surface microtopography of the fibers randomly picked from the solution. It reveals that the surface quality of the fiber seeds is closely related to their width. On prismatic faces of most fiber seeds wider than 10 μm (Fig. S2a), steps had already developed (Fig. 2a). The measured step height is 0.88 ± 0.05 nm, matching the interplanar spacing

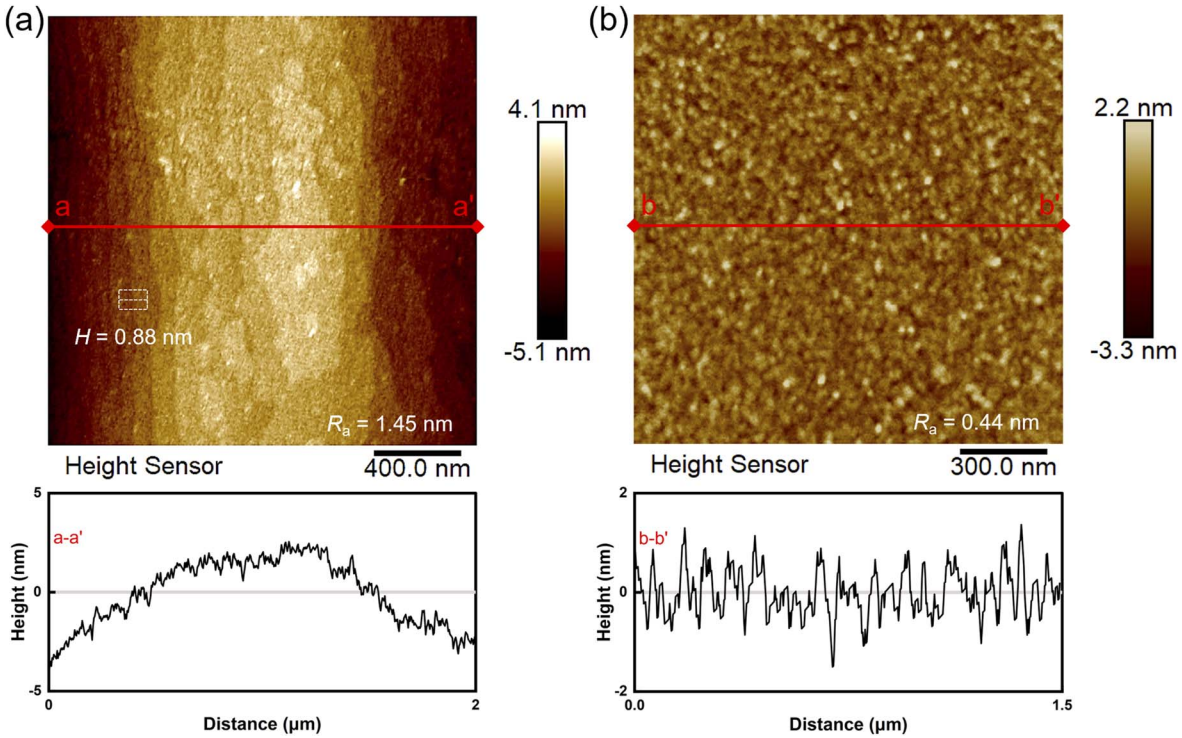


Fig. 2 AFM images and surface profiles of the spontaneously nucleated monoclinic KDP fiber seeds: (a) typical $W > 10$ μm and (b) typical $W < 10$ μm.

$d$ $(10\bar{2})$ ($\approx$0.88 nm) of the $(10\bar{2})$ facet from the Bravais–Friedel Donnay–Harker (BFDH) simulation.[26] Fig. 2a also shows the profile of this crystal surface with a $R_a$ roughness of 1.45 nm. In contrast, on the prismatic faces of fiber seeds thinner than 10 μm (Fig. S2b), no macroscopic defects, dislocations and growth steps were observed. Fig. 2b presents its AFM image and the surface profile obtained showing an extremely smooth surface with a $R_a$ roughness of 0.44 nm. Therefore, the crystal faces of most fiber seeds with a width ($W$) of less than 10 μm are smooth and defect-free, which is similar to the case of metallic whiskers with a diameter in microns, reported with a nearly perfect lattice structure.[34] This crystal growth phenomenon contradicts the viewpoint held by some researchers that the rapid growth in highly supersaturated solutions cannot yield perfect crystals.[35] In our experiment, high-quality metastable fibers can not only be produced through a rapid growth in a highly supersaturated solution at room temperature but also be successfully picked from a solution while maintaining structural stability over a long period of time under low-humidity conditions. These defect-free crystalline metastable KDP fiber seeds with smooth surfaces possess a high lattice mismatch with the stable tetragonal phase, which may increase the interfacial energy and raise the 2D nucleation barriers against such crystal transformation on the surface of the metastable crystal phase. Therefore, the quality of the crystal, particularly its surface integrity, effectively determines the phase stability of metastable crystals and enables smooth seeding and growth in solution without crystal transition. Furthermore, compared with spontaneous crystallization, seeded growth enables better controllability over the metastable crystal growth system. Crystal seeds provide nucleation sites that induce secondary nucleation and usually enable stable crystal growth in a lower supersaturation level than the spontaneous nucleation required in the metastable zone.[36–38] Therefore, seeding growth using defect-free seeds represent an effective approach for realizing controlled growth of metastable crystals.

### Determination of the solubility curve and 1D growth curve

Measurement of the solubility curve of metastable monoclinic KDP was performed using defect-free fiber seeds and carefully prepared stable, highly supersaturated solutions to reduce the tendency of crystal transition. The solubility was determined by observing the morphological evolution of the metastable fibers seeded into solutions with specific concentrations under dynamically changing temperature conditions. The critical state of the dissolution or crystallization of the fiber seeds was monitored *in situ* using a home-made microscopic imaging system (Fig. S3). The dissolution of the crystal indicates that the solution is undersaturated at the specified temperature. During the subsequent slow-cooling process, the temperature at which the dissolution ceases was experimentally defined as the saturation temperature ($T$). The saturation temperature represents the specific temperature at which the solution of a given concentration is in equilibrium with the solid phase, meaning that the solution is exactly saturated. Saturation temperatures were determined across a range of solution concentrations, and these obtained data were plotted and fitted to construct the solubility curve of monoclinic KDP:

$$C_e = 28.40858 + 0.38265T + 0.00586T^2 \text{ (g KDP/100 g } H_2O),$$

where $C_e$ is the equilibrium solubility and $T$ is the saturation temperature of the solution (the independent variable obtained from the experiment and analyzed *via* the fitting procedure). According to the above experiment, the solubility of the metastable monoclinic KDP at room temperature (25 °C) is 42 ± 0.3 g KDP/100 $H_2O$, corresponding to $S_T = 1.49 \pm 0.01$. This solubility value of the metastable monoclinic KDP crystal measured at 25 °C is lower than that reported by Cedeno *et al.*, (45 ± 2 g KDP per 100 g water).[23] This discrepancy may be partly attributed to differences in crystal quality, as defect-free crystals generally have a higher saturation temperature than defective ones. The supersaturation values ($\sigma_M$) relative to the metastable monoclinic KDP under varied solution conditions could be calculated based on the fitted equation (Table S1). By further decreasing the temperature to a critical point, the one-dimensional (1D) growth of the metastable KDP SCF was initiated. These critical temperatures obtained in different concentrations were further fitted to generate the 1D growth curve of KDP fiber seeds.

### Growth regions for the stable and metastable KDP phases

To determine the thermodynamic conditions under which the stable and metastable crystal phases of KDP can exist and grow, the solubility and 1D growth curves of both crystalline phases were plotted in the same temperature-*versus*-solution concentration graph for comparison (Fig. 3). The thermodynamic data related to the tetragonal phase of KDP presented in this work were derived from previous studies by our research group.[27] Clearly, a significant solubility difference existed between the stable tetragonal phase and the metastable monoclinic phase. The solubility of the tetragonal phase was 25 ± 0.3 g KDP/100 g $H_2O$ at 25 °C, and the solubility of the monoclinic phase was approximately 1.68 times higher than that of the tetragonal phase. The fundamental reason for the higher solubility of the metastable phase than its stable counterpart lies in its higher Gibbs free energy.[39,40] Thermodynamically, the stable phase corresponds to the lowest Gibbs free energy of the system, whereas the metastable phase occupies a local minimum on the energy landscape, possessing a higher Gibbs free energy relative to the stable phase. This additional free energy lowers the barrier for molecules to escape the solid lattice and enter the solution, thereby leading to the higher solubility of the metastable phase. The difference in solubility between the two crystalline phases also explains why the crystal transition of the metastable monoclinic phase into the tetragonal phase occurs once the latter nucleates around the former in the solution, as shown in Fig. 1f. As can be seen from Fig. 3, four curves delineate three characteristic dissolution-growth regions. Region I is the undersaturated area, where both crystal phases dissolve. Region II is characterized by supersaturation with respect to the tetragonal phase and undersaturated with respect to the monoclinic phase. In this area, only the tetragonal crystals can be grown from the solution. Defect-free fiber seeds allow us to capture the distinct morphological changes exhibited by the two phases in this region. Specifically, when the crystals of both phases were seeded simultaneously at the location marked by the black asterisk in Fig. 3, the monoclinic fiber slowly dissolved while the tetragonal fiber grew rapidly (see SI Movie 2). Region III is supersaturated for both tetragonal and monoclinic phases, and crystals of both phases could grow within this region. It is noteworthy that the solution condition triggering crystal growth of the monoclinic phase corresponds to an extremely high supersaturation for the tetragonal phase (Table S1). Within the stable region of the tetragonal phase in region III, however, it is possible to realize the controlled metastable growth of the monoclinic SCFs using defect-free fiber seeds in a high-purity solution. Based on the preceding experimental results, the monoclinic KDP crystals tend to nucleate preferentially in regions where the supersaturation ratio exceeds 2.99. At $S_T < 2.96$ in region III, in principle, the tetragonal phase is more likely to crystallize. The growth curve of the monoclinic phase shows that it can co-exist metastably within the stability region where the tetragonal phase nucleates preferentially. Moreover, there exists a relatively broad growth zone for the stable growth of the metastable phase in the system. This zone extends from the initiation growth temperature point of the monoclinic phase to its preferential crystallization temperature, with a coverage of at least 30 °C, and within this zone, a stable growth of the metastable monoclinic crystals can be achieved. This is similar to the case of the widely reported metastable phase growth of DKDP crystals (the deuterated isotopic compound of KDP crystals). Under high supersaturation conditions, high-quality metastable tetragonal DKDP crystals were grown over a wide temperature range that falls within the stability region of the DKDP monoclinic phase.[41]

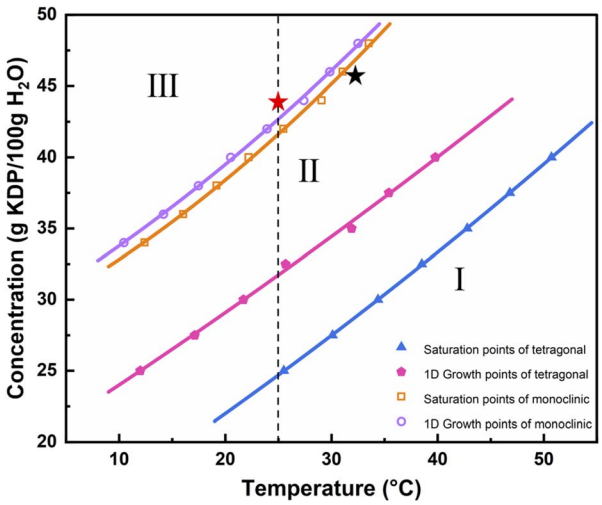


Fig. 3 Solubility and 1D growth initiating curves of the tetragonal and monoclinic KDP fibers ($W = 5.0 \pm 1.5$ μm), and the three characteristic dissolution/growth regions (I–III). Dotted lines: varying supersaturation conditions at room temperature (25 °C) for studying the morphological evolution of tetragonal and monoclinic fiber seeds, black asterisks: undersaturation and red asterisks: supersaturation relative to the monoclinic phase solubility.

### Growth kinetics of the metastable crystal phase

Compared with the thermodynamic growth conditions of polymorphs, the growth kinetics of metastable crystal phases have received considerably less attention, and available experimental data remain relatively scarce.[19] However, they play an equally crucial role in guiding crystal growth. Real-time *in situ* observations of the crystal growth of SCFs were conducted, and kinetic data were concurrently collected. Fig. 4a presents the typical growth rate curve of a 4.5-μm-wide monoclinic fiber seed in a solution with $\sigma_M = 3.47\%$. The growth rate initially increases sharply, then rises gradually, and ultimately plateaus with prolonged growth time. This is because when the solution is stationary, the crystal faces grow at a rate determined by the molecular diffusion of the solute to the crystal. The growth rate increases with the flow velocity of the solution towards the crystal. However, due to the presence of diffusion limitations,[32] this growth rate gradually approaches to saturate, reaching the upper limit determined by the crystal surface kinetics. The same trends of growth rate *versus* time can be observed for monoclinic KDP SCFs grown in other supersaturated solutions. The variation of the growth rate with crystal width was also evaluated, as shown in Fig. 4b. The results indicate that the crystal growth rate decreases exponentially with the increase in fiber width. This characteristic further indicates that a sufficient mass transfer at the crystal tip of thinner SCFs with a smaller cross-sectional area promotes their rapid growth compared with thicker ones. Thicker SCFs are even likely to form hollow crystals as a result of insufficient solute transport induced by the tip diffusion limitation. This phenomenon is particularly prominent in thicker crystals with initiated prismatic faces. Furthermore, the dependence of the 1D growth rates of the monoclinic SCF on supersaturation was determined, as

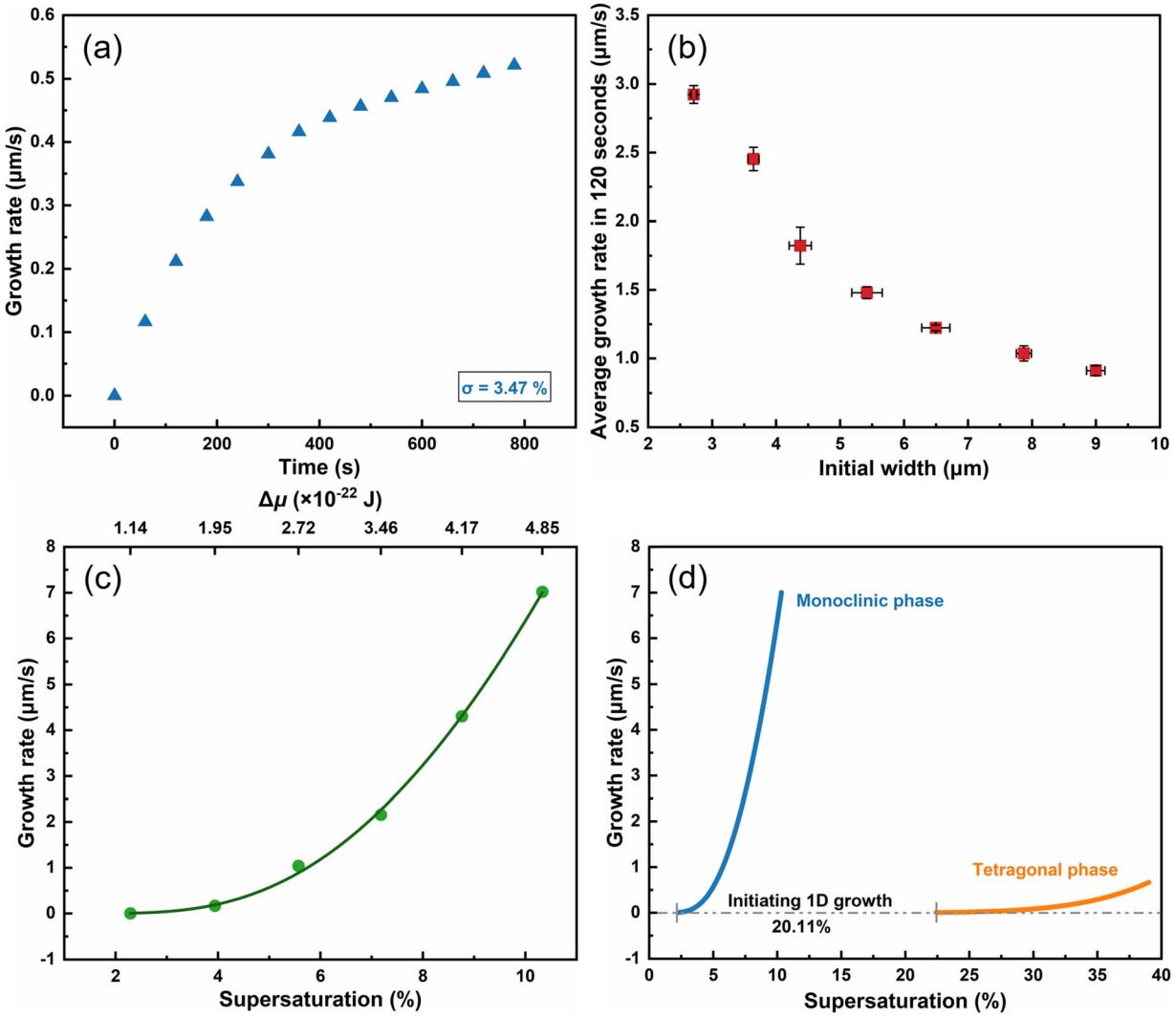


Fig. 4 Growth kinetics of the metastable monoclinic phase of KDP: (a) time-dependent growth rate curve of monoclinic KDP SCF in a solution with 3.47% supersaturation, (b) average growth rate of monoclinic KDP SCFs with different initial widths over a period of 120 s, (c) 1D growth rate of monoclinic KDP SCF *versus* the supersaturation and $\Delta\mu$ (solid lines are the fitting curves). (d) Comparison of the growth kinetics of monoclinic (blue, $W = 4.5$ μm) and tetragonal (orange, $W = 2.3$ μm) KDP SCFs *versus* supersaturation, with a 20.11% difference in the supersaturation required for initiating their 1D growth.

illustrated in Fig. 4c, with the corresponding growth driving force ($\Delta\mu$) provided on the top axis. The curve fitting results indicate that the 1D growth rate of the SCF increases exponentially with the increase in supersaturation. The functional relationship between growth rate and supersaturation is fully consistent with the typical 2D nucleation normal growth rate function:[42]

$$R = C_1 \times \sigma^{2/3}[\ln(1+\sigma)]^{1/6} \exp\{-C_2/[T^2 \times \ln(1+\sigma)]\},$$

where $R$ denotes the normal growth rate of the crystal face (μm $s^{-1}$); $\sigma$, the relative supersaturation (dimensionless); $T$, the temperature (K); and $C_1$ and $C_2$, the kinetic coefficients (μm $s^{-1}$), confirming the 2D nucleation growth of the metastable KDP crystals (see fitting accuracy and kinetics coefficients in Table S2).

The difference in solubility between these two crystalline phases results in distinct supersaturation levels at a given solution concentration. Fig. 4d presents the exponential fitting curves of the growth rates *versus* supersaturation for the tetragonal and monoclinic phases of KDP, respectively. The result clearly indicates that the metastable monoclinic phase requires a lower supersaturation, or a smaller growth-driving force, to initiate 1D growth, yet it exhibits a higher overall growth rate. This indicates that the two crystal phases have different specific edge energies for 2D nucleation. Compared with the stable phase, the lower edge energy of the metastable phase reduces the barrier for 2D nucleation, thereby accelerating growth. This inference is supported by the classical nucleation theory (CNT). Under conditions of smooth crystal face and growth dominated by 2D nucleation, the crystal growth rate ($R$) is proportional to the 2D nucleation rate ($J$), with both quantities following the relationship $R \propto J \propto \exp(-\Delta G^*_{2D}/k_B T)$, where $\Delta G^*_{2D}$ denotes the 2D nucleation barrier and $k_B$ represents Boltzmann's constant.[43,44] As the nucleation barrier is proportional to specific edge energy, $\Delta G^*_{2D} = \Omega\pi\gamma^2 h/\Delta\mu$, where $\Omega$ is the volume per structural unit, $\gamma$ is the specific edge free energy, and $h$ is the height of the 2D crystal nucleus.[42] It is reasonable to believe that the low specific edge energy of 2D nucleation results in a higher nucleation and growth rate on smooth crystal faces. On the other hand, high growth rate is certainly closely related to the unique crystal structure of the individual crystals. The high specific edge energy on the pyramidal faces of the metastable SCF may play a key role in increasing its 1D growth rate. However, quantitatively assessing the specific edge energy of metastable phases remains a significant challenge, necessitating future research aimed at elucidating these critical parameters through combined experimental and theoretical approaches.

### Morphology-controlled growth of metastable KDP crystals

Further investigation was conducted on the morphology-controlled growth of the metastable monoclinic phase of KDP. As shown in Fig. 5a, the supersaturation zones for the one-dimensional and three-dimensional (3D) growth of both the stable and metastable crystalline phases at 25 °C were clearly delineated (corresponding to the dotted lines indicated in Fig. 3). Two distinctive phenomena were observed. One is that when the supersaturation is higher than the critical point to initiate growth on fiber seeds, the crystal faces do not start growing simultaneously. At room temperature (25 °C), the critical supersaturation governing the growth of the tip faces of the metastable monoclinic SCF was measured to be 2.29%, which is equivalent to a supersaturation relative to the tetragonal phase of $\sigma_T = 51.82\%$ (Fig. S4). When $\sigma_M > 11.87\%$ (equivalent to $\sigma_T > 66.04\%$), the prismatic faces of the monoclinic SCF start to grow (Fig. S5). This phenomenon is also associated with the variations in the 2D nucleation barriers. As revealed by AFM microtopography (Fig. 2), the surfaces of the micron-sized high-quality seed crystals are defect-free and have no dislocations. To initiate 2D nucleation growth on such smooth crystal faces, it is necessary to overcome a certain high-nucleation barrier under high supersaturation. Due to anisotropy, different crystal faces possess different surface energies. Compared with the prismatic faces, the tip faces of the microscale-width KDP SCFs have higher surface energies,[45] which result in a lower energy barrier for 2D nucleation and faster growth rate.[46,47] Therefore, when a certain supersaturation level is reached, growth is first initiated at the tip of the fiber seed. The prismatic faces start to grow at a higher supersaturation level. The supersaturation difference between the initiation of 1D and prismatic growth spans a wide supersaturation range. This characteristic allows control of the crystal growth morphology by seeding at different supersaturation levels, thereby obtaining metastable KDP crystals with different aspect ratios. Another feature is that the critical supersaturations required to initiate 1D and 3D growth for monoclinic and tetragonal fiber seeds are significantly different. As is clearly observed in Fig. 5a, the critical supersaturation required for the 1D growth of the tetragonal phase at 25 °C is approximately 9.8 times that of the monoclinic phase, while the value for prismatic growth is approximately 3.5 times the latter. This suggests that the driving force required to initiate the growth of KDP's metastable monoclinic phase, as well as its 2D nucleation barrier, is likely lower than that of the stable tetragonal phase. When the fiber crystal seeds of both phases were simultaneously seeded into the solution at $\sigma_M = 3.94\%$ ($\sigma_T = 54.27\%$, marked by a red asterisk in Fig. 3), both phases exhibited high growth rates. Specially, while the monoclinic phase maintains a 1D growth, the tetragonal phase has already initiated the growth of its prismatic faces (see SI Movie 3). Two crystal phases were then verified *via* XRD analysis (Fig. 5b), and no crystal transition was observed after they were simultaneously seeded and grown in the above solution.

Overall, although the monoclinic KDP SCFs are not a thermodynamically stable phase, their defect-free quality combined with high 2D nucleation barriers on smooth surfaces hinders crystal transformation into the stable tetragonal phase, thereby enabling their long-term relative stability. Additionally, as shown in the schematic diagram (Fig. 5c), metastable defect-free fiber seeds help achieve high growth rate and effective morphological control. By seeding high-quality metastable fiber seeds in different supersaturation regions, the fully controllable 1D and 3D growth of KDP monoclinic single crystals was

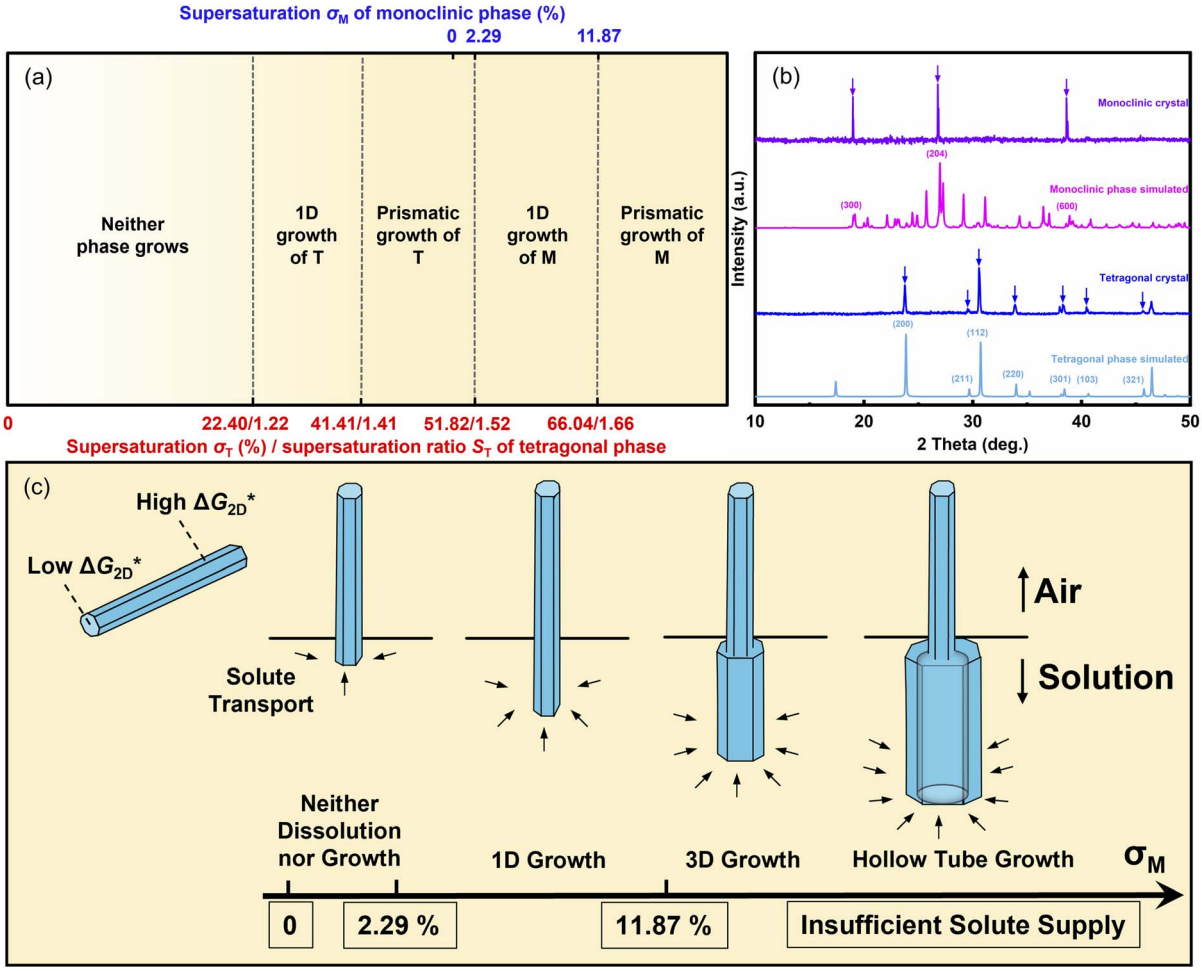


Fig. 5 (a) Supersaturation ranges for the 1D and 3D growth of tetragonal (T) and monoclinic (M) KDP fiber seeds obtained by seeding at room temperature (25 °C) (blue top axis: supersaturation ($\sigma_M$) for the monoclinic phase; red bottom axis: supersaturation ($\sigma_T$)/supersaturation ratio ($S_T$) relative to the tetragonal phase). (b) XRD patterns of the tetragonal and monoclinic crystals after being simultaneously seeded into an $\sigma_M = 3.94\%$ solution and grown. (c) Schematic of the morphological evolution from 1D fibrous to 3D rod-like growth in a monoclinic KDP fiber seed.

realized, achieving distinct crystal morphologies. In the supersaturation range of $\sigma_M$ = 2.29–11.87%, a seeded growth produces fibrous crystals of up to centimeters in length exclusively *via* 1D growth (Fig. 6a). As shown in Fig. 6b, these metastable single-crystal fibers exhibit remarkable flexibility. They can be coiled into loops with a curvature radius ($\rho$) of as small as about 50 μm without fracture. Notably, this bending deformation is fully reversible; the fiber recovers its original straight morphology upon release, even after being maintained in the bent state for extended periods (at least two months). The ability

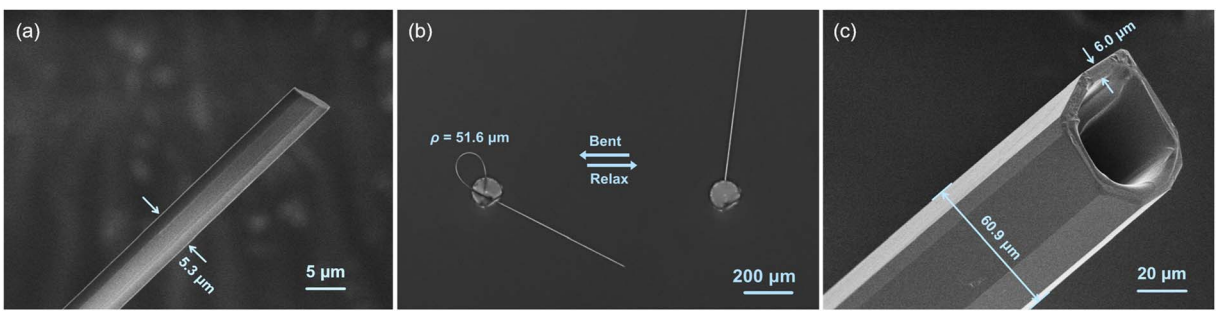


Fig. 6 (a) SEM image of a monoclinic single-crystal fiber ($W = 5.3$ μm) grown at $\sigma_M = 5.57\%$. (b) Coiling and elastic recovery of a monoclinic KDP SCF on a silica optical fiber, with a curvature radius of 51.6 μm when coiled. (c) SEM image of a monoclinic hollow tube ($W = 60.9$ μm) grown at $\sigma_M$ = 13.39%.

to withstand such a large elastic deformation indicates high fracture toughness, reflecting high structural integrity, which are all desirable traits for integration into flexible micro-optoelectronic devices. In a solution with $\sigma_M > 11.87\%$, monoclinic fiber seeds initiate growth on their prismatic faces, developing into three-dimensional rod-like crystals. Hollow tubular structures (diameters: tens to hundreds of micrometers) form in an extremely high supersaturation, where rapid growth on both the side and tip faces leads to a local shortage of solute supply at the advancing tip (Fig. 6c). The critical supersaturation boundary between solid rod and hollow tube growth has not yet been clearly defined as it depends on several factors, such as seed width, growth rate, and supersaturation. A systematic study of their formation mechanism is warranted in the future, considering their promising potential in optoelectronic applications.[48]

## Conclusions

In summary, by employing micron-sized, defect-free 1D crystal seeds *via* a solution-seeding approach, we effectively suppressed the solution-mediated crystal transformation. This enabled the accurate determination of the growth thermodynamics and kinetics of the metastable KDP phase. The distinct growth zones of the stable and metastable phases were determined. At $\sigma_M > 2.29\%$ (equivalent to $\sigma_T > 51.82\%$), the monoclinic phase could metastably exist and grow within the stability region of the tetragonal phase of KDP. The growth kinetics data revealed that the metastable monoclinic phase of KDP exhibits a lower 2D nucleation barrier for 1D growth and a higher growth rate compared with the stable tetragonal phase. Finally, by regulating the supersaturation of the solution, controlled growth of the metastable monoclinic crystals with different morphologies (single-crystal fibers, solid rods and hollow tubes) was successfully realized. This work provides a methodology for using defect-free crystal seeds to investigate the thermodynamics and kinetics of metastable phases and realize their controlled crystal growth. This approach is expected to facilitate the development of metastable functional crystals with tailored morphologies for advanced device applications.

## Author contributions

Dedication and conceptualization: Y. R.; methodology: C. L., C. Z., and Y. R.; investigation: C. L.; resources: Y. R.; writing – original draft: C. L.; writing – reviewing and editing: Y. R. and C. Z.; supervision: Y. R. and funding acquisition: Y. R.

## Conflicts of interest

There are no conflicts to declare.

## Data availability

The data supporting this article have been included as part of the supplementary information (SI). Supplementary information: crystal micrographs, solubility measurement data, supersaturation calculation formulae, experimental errors, and fitting parameters. See DOI: https://doi.org/10.1039/d5ra09916a.

## Acknowledgements

This work was financially supported by the National Natural Science Foundation of China (Grant No. 51872163) and Natural Science Foundation of Shandong Province (Grant No. ZR2019MEM006).

## References

1 R. Šuminas, G. Tamošauskas, G. Valiulis and A. Dubietis, *Opt. Lett.*, 2016, **41**, 2097–2100.
2 Y.-H. Song, J. Ge, L.-B. Mao, K.-H. Wang, X.-L. Tai, Q. Zhang, L. Tang, J.-M. Hao, J.-S. Yao, J.-J. Wang, T. Ma, J.-N. Yang, Y.-F. Lan, X.-C. Ru, L.-Z. Feng, G. Zhang, Y. Lin, Q. Zhang and H.-B. Yao, *Sci. Adv.*, 2022, **8**, eabq2321.
3 A. Ashok, A. Vasanth, T. Nagaura, C. Setter, J. K. Clegg, A. Fink, M. K. Masud, M. S. Hossain, T. Hamada, M. Eguchi, H.-P. Phan and Y. Yamauchi, *J. Am. Chem. Soc.*, 2023, **145**, 23461–23469.
4 A. Nie, Z. Zhao, B. Xu and Y. Tian, *Nat. Mater.*, 2025, **24**, 1172–1185.
5 N. Blagden, M. de Matas, P. T. Gavan and P. York, *Adv. Drug Delivery Rev.*, 2007, **59**, 617–630.
6 M. Maruyama, H. Y. Yoshikawa, K. Takano, M. Yoshimura and Y. Mori, *J. Cryst. Growth*, 2023, **602**, 126990.
7 Q. Shao, Y. Wang, S. Yang, K. Lu, Y. Zhang, C. Tang, J. Song, Y. Feng, L. Xiong, Y. Peng, Y. Li, H. L. Xin and X. Huang, *ACS Nano*, 2018, **12**, 11625–11631.
8 T. K. Gupta, F. F. Lange and J. H. Bechtold, *J. Mater. Sci.*, 1978, **13**, 1464–1470.
9 H. Guo, H. Ping, J. Hu, X. Song, J. Zheng and F. Pan, *J. Mater. Chem. A*, 2017, **5**, 14294–14300.
10 D. B. Trushina, T. V. Bukreeva, M. V. Kovalchuk and M. N. Antipina, *Mater. Sci. Eng., C*, 2014, **45**, 644–658.
11 P. Dandekar, Z. B. Kuvadia and M. F. Doherty, *Annu. Rev. Mater. Res.*, 2013, **43**, 359–386.
12 Y. Du, C. Zhao, S. Li, T. Dai, X. Yang, Y. Zhu and Q. Shao, *Chem. Soc. Rev.*, 2025, **54**, 7706–7739.
13 Y. Zhang, Y. Li, Y. Chen, X. Xu, Z. Li, T. Zhang, W. L. Ong, S. M. Kozlov, Z. Zou, G. W. Ho and Z. Li, *Mater. Today*, 2025, **90**, 598–628.
14 W. Ostwald, *Z. Phys. Chem.*, 1897, (22U), 289–330.
15 J. Nývlt, *Cryst. Res. Technol.*, 1995, **30**, 443–449.
16 T. Threlfall, *Org. Process Res. Dev.*, 2003, **7**, 1017–1027.
17 K. Sato, *J. Phys. D: Appl. Phys.*, 1993, **26**, B77.
18 N. Doki, M. Yokota, K. Kido, S. Sasaki and N. Kubota, *Cryst. Growth Des.*, 2004, **4**, 103–107.
19 P. Sacchi, P. Neoptolemou, R. J. Davey, S. M. Reutzel-Edens and A. J. Cruz-Cabeza, *Chem. Sci.*, 2023, **14**, 11775–11789.
20 T. A. Land, T. L. Martin, S. Potapenko, G. T. Palmore and J. J. De Yoreo, *Nature*, 1999, **399**, 442–445.
21 Y. Ren, X. Zhao, E. W. Hagley and L. Deng, *Sci. Adv.*, 2016, **2**, e1600404.

22 S. Lee, H. S. Wi, W. Jo, Y. C. Cho, H. H. Lee, S.-Y. Jeong, Y.-I. Kim and G. W. Lee, *Proc. Natl. Acad. Sci. U. S. A.*, 2016, **113**, 13618–13623.
23 R. Cedeno, R. Grossier, N. Candoni and S. Veesler, *Cryst. Growth Des.*, 2023, **23**, 9052–9057.
24 Y. C. Cho, S. Lee, L. Wang, Y.-H. Lee, S. Kim, H.-H. Lee, J. J. Lee and G. W. Lee, *Nat. Commun.*, 2024, **15**, 3117.
25 Y. C. Cho, L. Wang, Y.-H. Lee and G. W. Lee, *Cryst. Growth Des.*, 2024, **24**, 8345–8353.
26 C. Li, Q. Bao, J. Song, C. Zhang and Y. Ren, *ACS Omega*, 2025, **10**, 39073–39080.
27 C. Li, X. Liu, Z. Gao, J. Song, C. Zhang and Y. Ren, *Inorg. Chem.*, 2023, **62**, 19159–19163.
28 W. K. Burton, N. Cabrera and F. C. Frank, *Philos. Trans. R. Soc. London, Ser. A*, 1951, **243**, 299–358.
29 M. Uwaha, *Prog. Cryst. Growth Charact. Mater.*, 2016, **62**, 58–68.
30 K. N. Olafson, J. D. Rimer and P. G. Vekilov, *Phys. Rev. Lett.*, 2017, **119**, 198101.
31 N. Kubota, M. Kobari and I. Hirasawa, *Advances in Organic Crystal Chemistry*, Springer Japan, Tokyo, 2015.
32 P. G. Vekilov, *Cryst. Growth Des.*, 2007, **7**, 2796–2810.
33 K. Itoh, T. Matsubayashi, E. Nakamura and H. Motegi, *J. Phys. Soc. Jpn.*, 1975, **39**, 843–844.
34 H. K. Hardy, *Prog. Met. Phys.*, 1956, **6**, 45–73.
35 D. Bonn and N. Shahidzadeh, *Proc. Natl. Acad. Sci. U. S. A.*, 2016, **113**, 13551–13553.
36 Z. Q. Yu, J. W. Chew, P. S. Chow and R. B. H. Tan, *Chem. Eng. Res. Des.*, 2007, **85**, 893–905.
37 Y. He, Z. Gao, T. Zhang, J. Sun, Y. Ma, N. Tian and J. Gong, *Org. Process Res. Dev.*, 2020, **24**, 1839–1849.
38 F. Zhang, B. Shan, Y. Wang, Z. Zhu, Z.-Q. Yu and C. Y. Ma, *Org. Process Res. Dev.*, 2021, **25**, 1496–1511.
39 D. Mangin, F. Puel and S. Veesler, *Org. Process Res. Dev.*, 2009, **13**, 1241–1253.
40 J. Xu, A. Li, W. Gao, M. Lu and L.-F. Ning, *J. Mol. Struct.*, 2025, **1338**, 142271.
41 M.-h. Jiang, C.-s. Fang, X.-l. Yu, M. Wang, T.-h. Zheng and Z.-s. Gao, *J. Cryst. Growth*, 1981, **53**, 283–291.
42 X. Y. Liu, K. Maiwa and K. Tsukamoto, *J. Chem. Phys.*, 1997, **106**, 1870–1879.
43 A. A. Chernov, *Modern Crystallography III*, Springer, Berlin, 1984.
44 I. V. Markov, *Crystal Growth for Beginners*, World Scientific Publishing Company, California, 2016.
45 X. Zhao, Y. Li and X. Zhao, *Molecules*, 2022, **27**, 9014.
46 Y. He, T. Yanagida, K. Nagashima, F. Zhuge, G. Meng, B. Xu, A. Klamchuen, S. Rahong, M. Kanai, X. Li, M. Suzuki, S. Kai and T. Kawai, *J. Phys. Chem. C*, 2013, **117**, 1197–1203.
47 X. Lu, X. Wang, Q. Liao and H. Fu, *J. Phys. Chem. C*, 2015, **119**, 22108–22113.
48 R. E. da Silva, J. H. Osório, G. L. Rodrigues, D. J. Webb, F. Gérôme, F. Benabid, C. M. B. Cordeiro and M. A. R. Franco, *Opt. Lett.*, 2024, **49**, 690–693.